Materials Advances

ROYAL SOCIETY OF CHEMISTRY

PAPER

View Article Online
View Journal | View Issue

Cite this: *Mater. Adv.*, 2024, 5, 9259

A mass spectrometrical surface chemistry study of aluminum nitride ALD from tris-dimethylamido aluminum and ammonia†

Pamburayi Mpofu, [a] Houyem Hafdi, [a] Jonas Lauridsen, [b] Oscar Alm, [b] Tommy Larsson [b] and Henrik Pedersen [a]*

Received 11th September 2024,
Accepted 28th October 2024

DOI: 10.1039/d4ma00922c

rsc.li/materials-advances

Dialkylamido compounds, such as tris-dimethylamido aluminum (TDMAA, $Al(NMe_2)_3$) and tetrakis-dimethylamido titanium (TDMAT, $Ti(NMe_2)_4$) are interesting precursors for depositing nitrides using atomic layer deposition (ALD) due to their high volatility and reactivity at low temperatures. In this study, we explored surface chemistry using mass spectrometry and discovered that the surface mechanisms involved β-hydride elimination and ligand decomposition, as well as transamination and hydrogenation reactions which facilitate ligand exchange. This is mainly based on the $-N(Me)_2$ and $HN(Me)_2$ detected during both TDMAA and NH_3 pulses, and CH_4 signals detected during the NH_3 pulse stage. The expected reductive elimination of the two dimethylamido ligands, *via* a direct nitrogen–nitrogen coupling reaction was not observed, suggesting that it is less thermodynamically favorable compared to reduction by NH_3. Arrhenius analysis between 150 and 300 °C found activation energies (E_a) = 27–30 kJ mol^{-1} and pre-exponential factors (A) = 3–5 s^{-1} for the reaction between TDMAA and NH_3.

1. Introduction

As atomic layer deposition (ALD) processes continue to be developed, the necessity for investigating reaction mechanisms remains important to understand both new reaction chemistries and existing processes. Thus, studying reaction mechanisms is crucial for identifying appropriate reactions to achieve desired materials and material combinations, especially as thin films in device structures reach thicknesses achievable within just a few ALD cycles.[1] The trend towards shrinking device dimensions necessitates, for example, the deposition of thinner films within higher aspect ratio holes and vias. In this context, ALD is an ideal method for depositing conformal films as it operates through two consecutive self-limiting reactions that take place between a gaseous precursor and the solid substrate, depositing a thin film through iteratively executing these surface reactions.

Aluminum nitride (AlN) is a wide-gap semiconductor known for its wide bandgap of around 6.2 eV,[2] a thermal conductivity comparable to that of metals of 285 W m^{-1} K^{-1}, a high melting point of 2750 °C, and electrical resistance of 10^{13} Ω cm, making it a highly promising material for utilization in micro- and optoelectronic applications.[3] ALD of AlN typically relies on trimethyl aluminum (TMA) and ammonia (NH_3) as precursors.[4,5] The deposition of AlN from TMA, with aluminum–carbon bonds, often suffers from carbon impurities and an efficient carbon-cleaning surface chemistry is needed.[6] Precursors with aluminum–nitrogen bonds could possibly reduce this problem when depositing AlN. The homoleptic amide precursor tris(dimethylamido)aluminum(III) ($Al(NMe_2)_3$, TDMAA), is therefore an interesting alternative, but it is less explored for ALD.[7] TDMAA has been used for AlN in thermal[8] and in plasma ALD[9] with NH_3 as a co-reactant but neither theoretical nor experimental surface reaction studies for ALD of AlN from TDMAA have been reported to date.

The dimethylamido ligand has been extensively used for ALD of titanium nitride (TiN) in the tetrakis(dimethylamido)-titanium(IV) ($Ti(NMe_2)_4$, TDMAT) precursor. TiN is a commonly employed diffusion barrier material[10] known for its hardness, refractory properties, and boasts a bulk resistivity of 20 μΩ cm.[3] The decomposition and reaction mechanisms of TDMAT have been extensively studied.[11–14] Another study on gas phase decomposition and reactions of different tris(dimethylamido) precursors, utilizing Fourier transform infrared spectroscopy and molecular beam mass spectrometry found that gas-phase decomposition of tris(dimethylamido)stibine (TDMASb) leads to the production of several stable products[15] including methylmethyleneimine (MMI), dimethylamine (DMA), and methane (CH_4).

[a] *Department of Physics, Chemistry and Biology, Linköping University, SE-581 83, Linköping, Sweden. E-mail: henrik.pedersen@liu.se*
[b] *Seco Tools AB, SE-737 82, Fagersta, Sweden*

† Electronic supplementary information (ESI) available. See DOI: https://doi.org/10.1039/d4ma00922c

These species are analogous to the pyrolysis of tris(dimethylamido)arsine (TDMAAs) and tris(dimethylamido)phosphine (TDMAP).[15] Therefore, one could hypothesize that TDMAA could have a similar gas phase chemistry to these precursors.

To the best of our knowledge, no earlier study has investigated or described a detailed reaction mechanism for TDMAA, making its surface chemistry less understood. Studies of other dimethylamido precursor can provide insights into the TDMAA surface chemistry. Hence, in this study, the surface chemistry of TDMAA for ALD of AlN was investigated for both plasma and thermal ALD, with NH_3 as the co-reactant, using mass spectrometry. Comparisons between TDMAA and TDMAT was also done to probe similarities between the possible reaction pathways of the two dimethylamido precursors.

2. Experimental details

A hot-wall Picosun R-200 Advanced ALD reactor, equipped with a Litmas remote inductively coupled plasma (ICP) source, was used for deposition. The reactor operated at 4 mbar with a continuous flow of 400 sccm high-purity N_2 (99.999% with further drying using a getter filter) into the chamber, which was also used as the purge gas. TDMAA and TDMAT from Sigma-Aldrich (both $\leq$ 100%) were sublimed at 120 °C and 60 °C respectively, and vapor was drawn by opening a valve to the low-pressure reactor. The thermal processes used NH_3 (AGA/Linde, 99.999% and further purified by a getter filter) as the nitrogen precursor whereas the plasma ALD processes used a plasma discharge in a mixture of 75 sccm NH_3 and 100 sccm Ar (99.999% and further purified by a getter filter). The ICP plasma source was located approximately 75 cm above the substrate and ignited the plasma with a 2800 W plasma power. Prior to deposition, approximately 2 cm × 2 cm Si(100) substrates were cleaned with acetone and isopropanol for 10 minutes each to remove surface contaminants before blow-drying them with N_2 gas. To avoid unwanted effects, the reactor was conditioned by doing long passivation runs of either nitrogen/NH_3 plasma or thermal treatment in N_2 flow for at least 24 hours while maintaining it at 4 mbar operating pressure and 150 °C on both substrate and wall temperature.

In situ quadrupole mass spectrometry (QMS) for gaseous species measurements was conducted using a Hiden Analytical HPR-30 residual gas analysis (RGA) vacuum process sampling system that includes a HAL 201 RC mass spectrometer in multiple ion detection (MID) mode and bar scan mode with the Faraday detector (source voltage for electron impact ionization set at 70 eV to ensure efficient reactant molecule fragmentation). The mass spectrometer is placed approximately 80 cm from the main reaction zone (substrate stage). It is important to acknowledge that the surface-generated species detected in the QMS analysis may arise from all surfaces in the reactor. Given that the reactor wall surfaces are relatively much larger than the substrate size, species originating from the walls can significantly impact the measured signal. To guarantee that all identified reaction products stem from reactions occurring at a consistent temperature, it is essential to maintain uniform temperatures across both the walls and substrate. In this study, temperatures were standardized at 150 °C to ensure that the measured reaction products were representative of reactions taking place.

The system was differentially pumped and the operating pressure during typical measurements is kept in the order of 10^{-6} mbar to enable mean free paths that allow collisionless particle transport of the ions from the orifice to the detector. The bar scan measurements covered a mass range of 1 to 50 atomic mass units (amu), which was suitable for detecting all relevant masses while maintaining a high scanning speed. To analyze the formation of reaction products and the utilization of reactant species, a series of MID measurements were carried out. The MID-scan involved five complete ALD cycles (both precursor and reactant pulses).

The measurement procedure for the process involved monitoring mass-to-charge (m/z) values in the same pressure ranges simultaneously. This monitoring encompassed three distinct sets of measurements: five 'background' ALD cycles with no precursor, co-reactant or plasma power turned on; five 'normal' plasma ALD cycles with both precursor and co-reactant and five 'normal' thermal ALD cycles. Selected m/z values were chosen from the bar scans to make up MID scans based on similar pressure ranges for easy comparison *e.g.*, grouping them as m/z = 15 and 16; m/z = 29 and m/z = 42, 43, 44 and 45. By structuring the measurement procedure in this manner, all sets of cycles were designed to induce similar pressure fluctuations as those experienced during a standard ALD cycle. This approach aimed to minimize any potential impact of pressure variations on the measured signal, ensuring a more accurate assessment of the process dynamics and reaction products. The obtained data was analysed using MASsoft 10 (Hiden Analytical) software.

3. Results

3.1. Film growth

Fig. 1 and 2 show that the TDMAA and NH_3 surface reactions are self-limiting, suggesting that reactions should produce atomic layer controlled growth of AlN films. The strong increase in growth per cycle (GPC) at temperatures above the temperature window for both plasma and thermal processes indicates that the deposition in those temperature regions is governed by a decomposition chemistry with a significant gas phase component, *i.e.*, decomposition of the TDMAA precursor. TDMAA is a dialkylamide precursor and since the thermal stability of dialkylamides is generally limited, substrate temperatures must be kept below the decomposition temperature.[16] For TDMAA, the decomposition temperature is at least 250 °C, if we consider data points outside of the temperature window where 'CVD-like' growth starts to occur (Fig. 1b and 2b). The growth rate of the AlN films was slightly above 1 Å per cycle for the plasma process and approximately 0.8 Å per cycle for the thermal process.

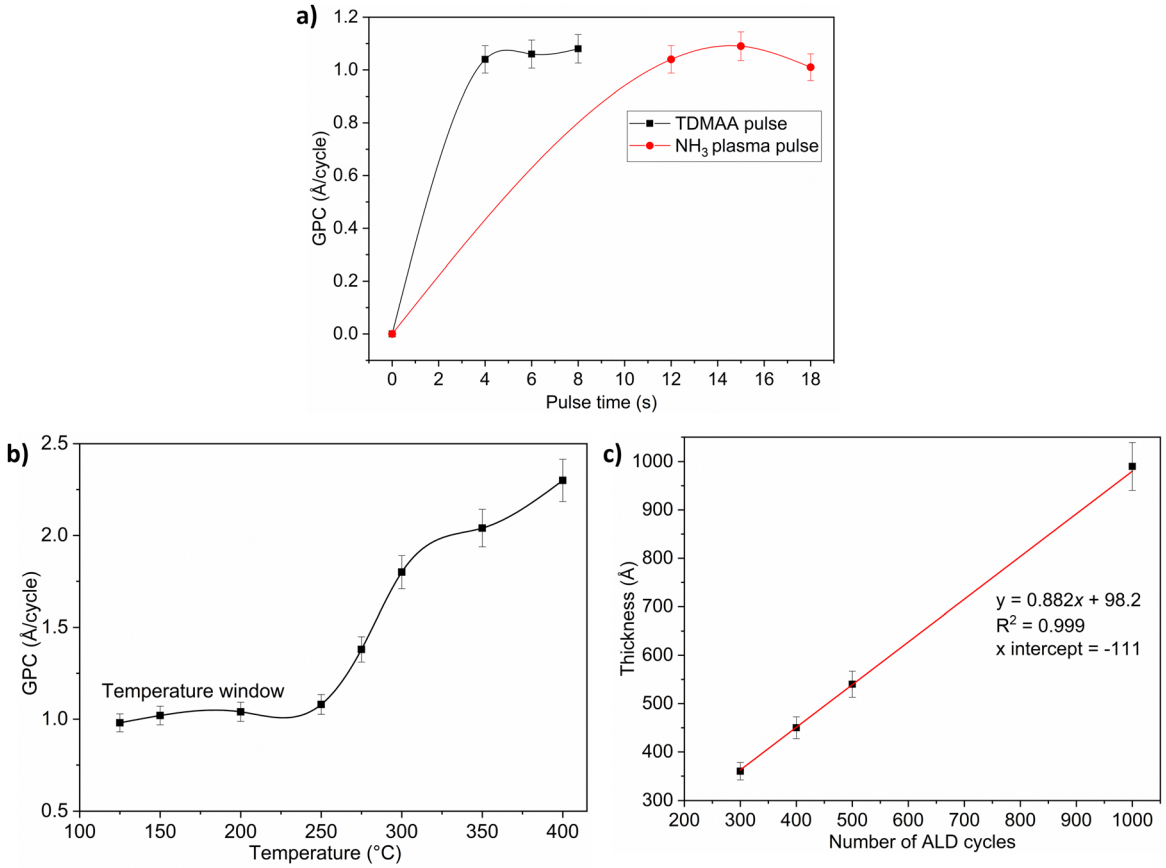

Fig. 1 Saturation curves for the plasma process, showing the effect of the TDMAA pulse time and the NH_3 plasma pulse time on the GPC (a). The plasma process growth dependence on process temperature is shown in (b) while film thickness dependence on number of cycles, showing no nucleation delay, for the plasma process is illustrated in (c).

Fig. 2(a) shows that the thermal process, just like the plasma process, has a low temperature window which is, however, slightly narrower.

The linear trend lines show that no incubation cycles are required before nucleation begins from ALD cycles *versus* film thickness in both processes (Fig. 1c and 2c). The fact that the fitted curve intersects the thickness axis above the origin suggests that the TDMAA based processes have substrate-enhanced growth. This can occur if the number of reactive sites on the substrate is higher than on the ALD grown film.[17,18] The GPC is then high at the very start of the deposition. For all processes, based on the respective saturation curves, 4 s pulse time for TDMAA was used while NH_3 pulse time was kept at 12 s.

3.2. Reaction products

Several species, summarized in Table 1, were detected during the ALD process as illustrated in Fig. 3. The main species included:

(i) Dimethylamine (NMe_2, DMA), *i.e.*, the intact ligand, with m/z = 44. The protonated ligand, *i.e.*, $HNMe_2$ with m/z = 45 was also detected.

(ii) *N*-Methyl methyleneimine ($CH_3N{=}CH_2$, MMI) with m/z = 43. MMI is a likely product from decomposition of the dimethylamido ligand.

(iii) Methane (CH_4) with m/z = 16. Methane can be released as a byproduct during the decomposition and reaction of TDMAA with NH_x species. The formation of methane may also occur through the cleavage of bonds within the TDMAA molecule, *i.e.*, ligand decomposition. It should be noted that nitride processes with NH_3 adds uncertainties to the interpretation of the m/z = 16 signal, as it can also be NH_2 from NH_3 decomposition/ fragmentation in the QMS.

Mass spectrometry species from an electron impact energy of 70 eV show that the detected ions primarily consisted of fragments from the effluent molecules, with no portion of the spectrum representing parent molecular ions. This is illustrated in Fig. 3 for both the plasma and thermal processes in comparison to the background where no parent precursor is pulsed.

DMA is characterized by known peaks at m/z = 45, 44, 30 ($HNCH_3^+$), and 15 (CH_3^+).[22] The presence of peaks at m/z = 28 ($N{=}CH_2^+$), 27, and 26 is indicative of *N*-methylmethaneimine (MMI, $CH_3N{=}CH_2$).[22] MMI can also be identified by the peak at m/z = 43 or 42 ($CH_2{=}N{-}CH_2^+$).[14] Additionally, a fraction of the peak at m/z = 15 (CH_3^+) may result from the fragmentation of MMI, a common byproduct from the decomposition of dimethylamido-metal precursors.[12,15,22,23] Therefore, in low-temperature ALD utilizing TDMAA, it is important to consider possible reactions in the gas phase or on the surface that

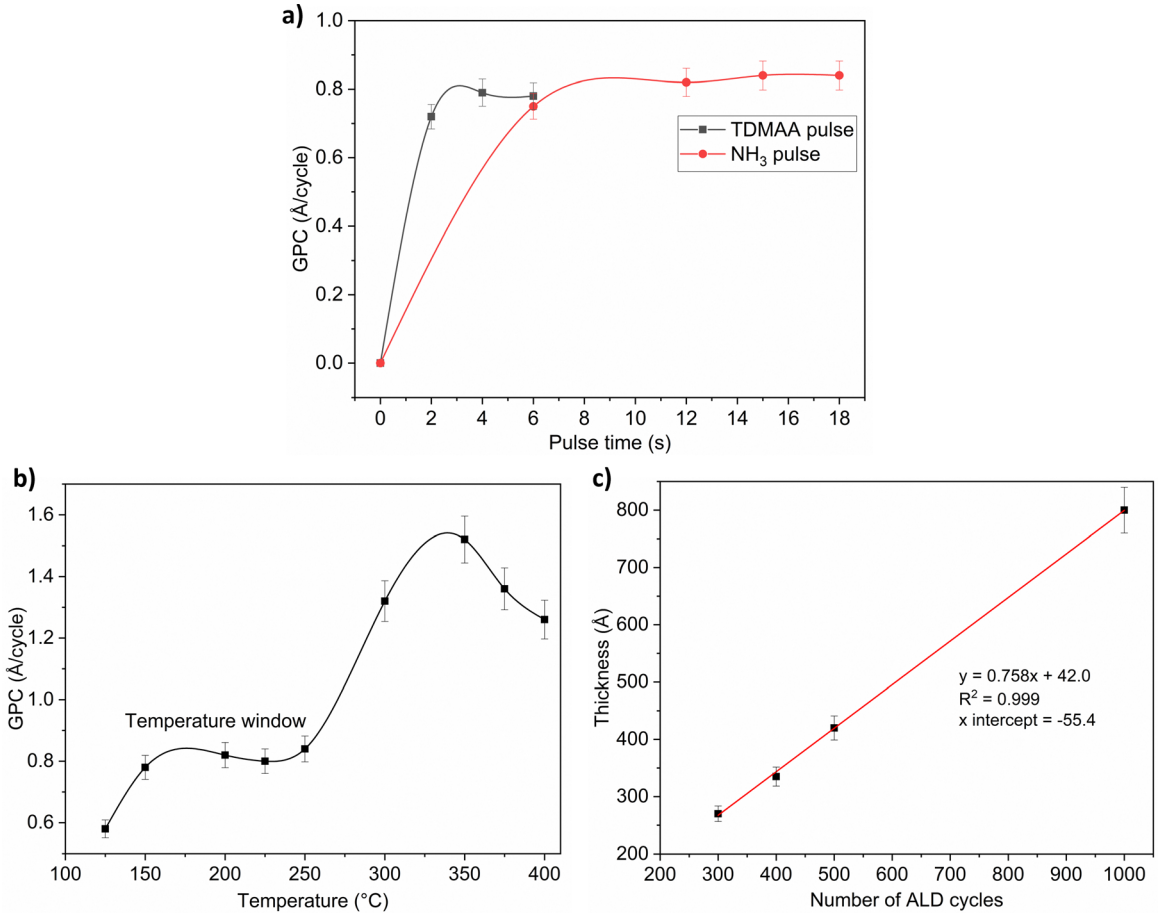

Fig. 2 Saturation curves for the thermal process, showing the effect of the TDMAA pulse time and the NH_3 pulse time on the GPC (a). The thermal process growth dependence on process temperature is shown in (b) while film thickness dependence on number of cycles, showing no nucleation delay, for the thermal process is illustrated in (c).

Table 1 Observed *m*/*z* signals from TDMAA, and their corresponding fragments

m/*z*	Fragment	Comment
2	H_2^+	Reaction product: NH_3 decomposition
14	$N^+/N_2^{2+}/CH_2^+$	Carrier gas/ligand decomposition
15	NH^+/CH_3^+	Co-reactant/ligand decomposition
16	NH_2^+/CH_4	Co-reactant fragmentation[5]/ligand decomposition[19]
17	NH_3^+	Co-reactant
18	H_2O^+	Residual water vapor: outgassing
27	HCN^+	Intermediate reaction product[20]
28	$N_2^+/N{=}CH_2^+$	Carrier gas/ligand decomposition
29	N_2^+/NCH_3^+	Co-reactant/ligand decomposition
30	$C_2H_6^+/HNCH_3^+$	Ligand decomposition
43	$(CH_2){=}N(CH_3)^+$	Disproportionation or decomposition reaction[14]
44	$N(CH_3)_2^+/CO_2^+$	Unprotonated ligand/ambient
45	$HN(CH_3)_2^+$	Protonated ligand, hydrogenation[21]

could result in the formation of MMI since MMI should be reactive towards the surface. The signal at *m*/*z* = 18 is assigned to H_2O^+, residual water vapor could be present in the reactor chamber given its background pressure of 4 hPa or introduced with the TDMAA precursor which was loaded in a stainless-steel container in a glove box but inserted in the ALD reactor in air. This handling could expose the TDMAA briefly to air. Although mass spectrometry data predominantly show DMA as a major product from the ligand, distinguishing between gas phase decomposition reactions and surface reactions poses a challenge. Competitive reactions could also result in the formation of additional byproducts such as MMI and CH_4 as will be explained later. Additionally, another species, hydrogen cyanide (HCN), was detected at *m*/*z* = 27 during the process, while cyanide (CN),

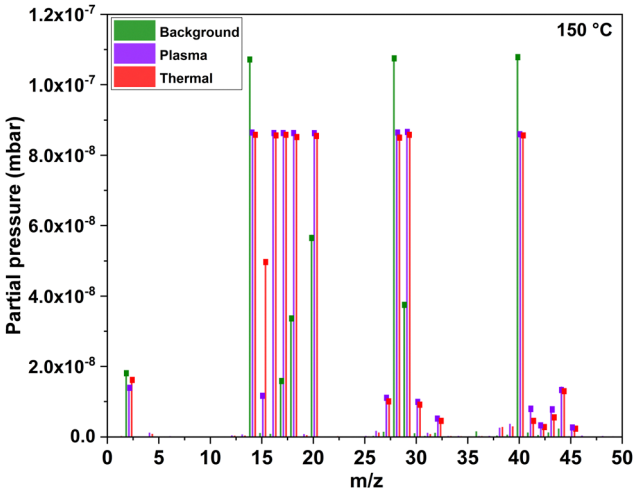

Fig. 3 Bar scan spectra showing the background (green) with no precursor, co-reactant or plasma power turned on and detected masses during ALD cycles when TDMAA and NH_3 were pulsed at 150 °C for the plasma (violet) and thermal (red) processes. Small mass offsets in m/z values on the horizontal axis were introduced for visual clarity.

reported as a decomposition product in ALD of TiN from TDMAT,[20] was not detected.

When time-resolving the evolution of reaction products from Fig. 3, DMA-related species m/z = 44 and m/z = 45 were initially chosen based on prior research and existing knowledge for alkylamido precursors.[24] This is illustrated in Fig. 4.

Evolution of selected additional significant intermediate species (m/z = 16 and 29 assigned to CH_4 and $HN{=}CH_2$ respectively) (Fig. 5), show that CH_4 is only released during the NH_3 pulse in both thermal and plasma processes while $HN{=}CH_2$ is released during the NH_3 pulse only in the plasma process.

3.3. Comparison to TDMAT

TDMAT is a well-studied precursor and has been used extensively for TiN deposition.[11,19,20,25–27] The suggested main decomposition mechanisms for TDMAT shown in Fig. 6 can be summarized as: (i) β-hydride elimination, where a hydrogen atom located on the β-carbon (adjacent to the Ti metal center) is eliminated. Subsequently, a double bond between the β-carbon and the adjacent atom is formed, resulting in the creation of hydride species and *N*-methyl methyleneimine ($CH_3N{=}CH_2$);[28] (ii) an intramolecular insertion metallacycle generation reaction[29] which results in the formation of a metallacycle Ti–C–N ring, that can participate in consecutive reactions and (iii) the transfer of a proton (transamination and hydrogenation)[19,21] to a dimethylamido group, leading to the formation of dimethylamine.

These species are formed as intermediates during the decomposition and reaction processes involving TDMAT on Si. Generation of methane (CH_4) during the gas phase decomposition of TDMAT at elevated temperatures (>350 °C) was proposed to be a gaseous radical disproportion reaction.[30]

We carried out a mass spectrometric survey scan to see the residual reaction species and by-products leaving the ALD reactor during TDMAT–NH_3 processes (Fig. 7a and b). The main residual species from the reactor (other than co-reactant NH_3, carrier gases N and Ar, and residual H_2O) are CH_4/NH_2, and the signals corresponding to m/z = 27, 29, 30, 42, 44 and 45. Considering that m/z = 44/45 to be the main reaction products, we studied and monitored their evolution with time as illustrated in Fig. 7c and d. It can be noted that both m/z = 44/45 signals are detected but with higher intensity during the NH_3 pulse compared to the TDMAT pulse. A similar observation was made during the TDMAA–NH_3 process.

4. Discussions

AlN growth from TDMAA and NH_3, is likely similar to the much more researched TDMAT and NH_3 for ALD of TiN.[14,31] We therefore did thermal- and plasma ALD experiments with TDMAT for comparisons to TDMAA. From the mass spectra in Fig. 7(a) and (b), we note prominent peaks around m/z = 44 signalling DMA as well as m/z = 16, 27, 29 and 30 which we also

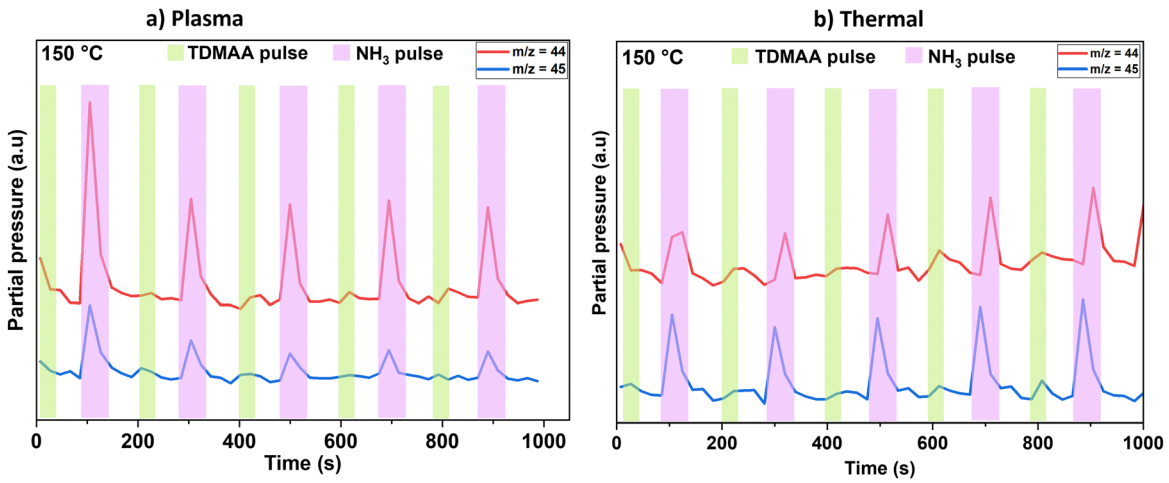

Fig. 4 Main reaction products (m/z = 44 and m/z = 45) created during the plasma (a) and thermal (b) processes at 150 °C probed and monitored over time by the mass spectrometer.

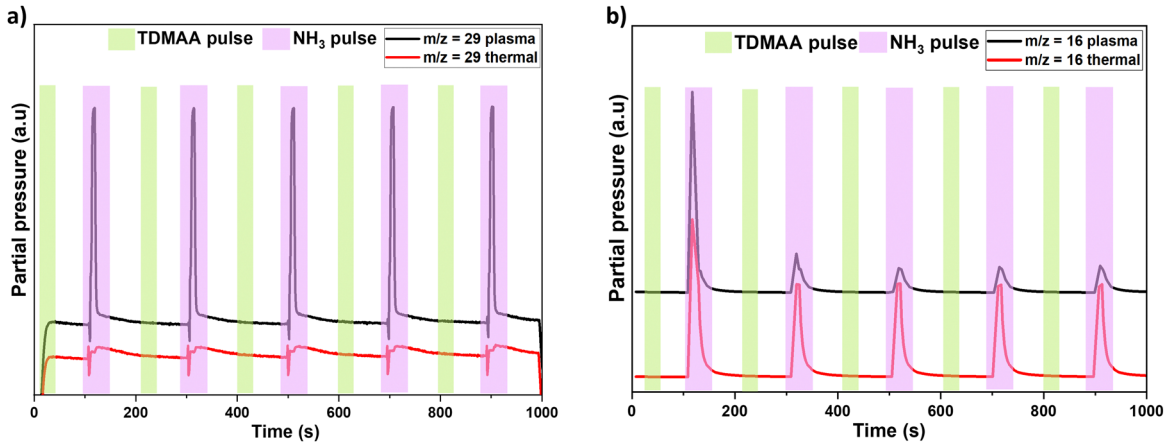

Fig. 5 Mass spectrometric time behaviour of other detected species m/z = 29 (a) and m/z = 16 (b), during five AlN growth cycles in plasma and thermal processes.

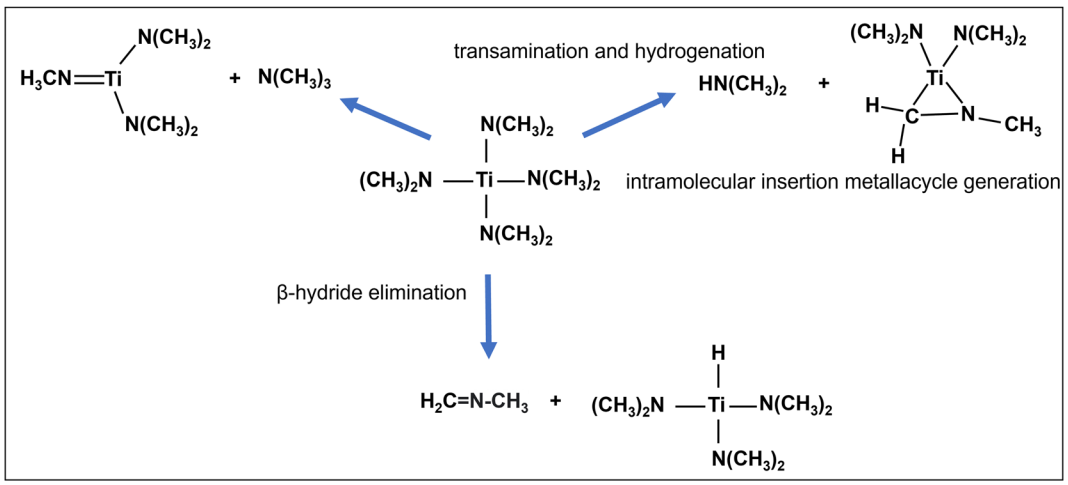

Fig. 6 The main proposed gas-phase decomposition pathways as applied to TDMAT.

identified in the TDMAA–NH_3 process. Looking at how TDMAT and TDMAA compare in the mass spectra, we believe that the reaction mechanisms for TDMAA are the same or at least very similar to the ones for TDMAT. In literature,[19] TDMAT has been suggested to decompose and react through an insertion-elimination reaction or a hydrogenation reaction leading to a transamination exchange, consisting of an attack on the Ti centre of TDMAT by the N lone electron pair of ammonia (H_2N–H). This reaction is characterized by elimination of $-N(CH_3)_2$ ligands at m/z = 44 or 45 (as dimethylamine) and insertion of ammonia (as NH_2) where a proton is transferred to a dimethylamido group, which leaves as dimethylamine.[19]

As was observed in TDMAA, complex surface reactions and intermediates do take place in TDMAT–NH_3 process as well, including the release of methane (m/z = 16) and signals at m/z = 27 and 30. However, the outstanding question at this point is the source of nitrogen in the deposited AlN films. There are two possible sources: TDMAA and NH_3. It is also important to note that results of TiN deposition with TDMAT and NH_3 as precursors, from isotopic labelling studies have concluded that all of the N in a 'clean' TiN thin film is derived from NH_3 *via* an intermolecular process[32] which facilitates transamination. We believe this could be the case as well for the TDMAA–NH_3 process, even though mass spectrometric results alone cannot drive us towards that same conclusion.

4.1. Reaction mechanisms

4.1.1. Main reaction products. Based on the main reaction product intensities monitored at 150 °C in Fig. 4, we propose that $HN(CH_3)_2$ is liberated both during the TDMAA pulse, and during the NH_3 pulse. This is supported by analogous results regarding the reaction mechanism in the plasma-assisted ALD process of TaN_x using similar ligand precursors, $Ta(NMe_2)_5$ and H_2 plasma[33] and thermal ALD of TiN from $Ti(NMe_2)_4$ and NH_3[27,34] and can be illustrated through transamination exchange reactions:

$$2\|\text{–NH}^{\bullet} + \text{Al(N(CH}_3)_2)_3 \rightarrow \|\text{–N}_2\text{AlN(CH}_3)_2{}^{\bullet} + 2\text{HN(CH}_3)_2\text{(g)} \quad (1)$$

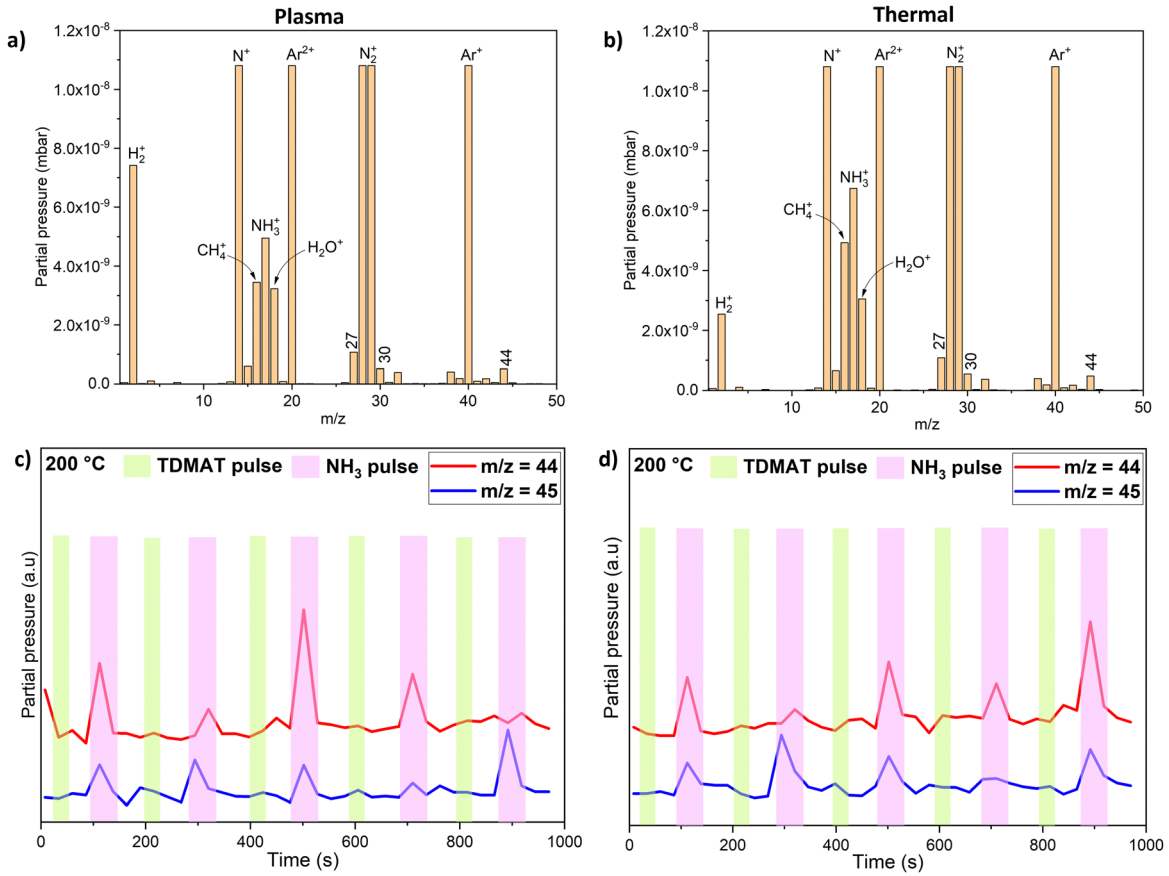

Fig. 7 Bar scan spectra showing detected masses during ALD cycles when TDMAT and NH_3 are pulsed at 200 °C during a plasma process (a) and a thermal process (b). Mass spectrometric time behaviour of detected $N(CH_3)_2$ (m/z = 44) and $HN(CH_3)_2$ (m/z = 45) during TiN growth from TDMAT and NH_3 at 200 °C for a plasma process is displayed in (c) while the thermal process is displayed in (d).

$$\|\text{–}N_2AlN(CH_3)_2^\bullet + 4/3(NH_3)(g) \rightarrow \|\text{–}N_2AlNH_2^\bullet + 2HN(CH_3)_2(g) + 1/6N_2(g) \quad (2)$$

Additionally, it has previously been suggested that the N–C bond on the ligand can only be broken at elevated temperatures, or by using plasma, leading to loss of the entire intact ligand.[15] The combination of a weak metal–N bond and high volatility in metal alkylamides generally facilitates effective deposition at lower temperatures.[22] Our results are in line with this as we only detect the assumed ligand decomposition product, NCH_3^+, with m/z = 29, during the NH_3 plasma pulse (Fig. 5a). This activation process is occasionally achieved using plasma[35] containing hydrogen, or nitrogen radicals (NH_3 plasma in this case). Presumably, NH_3 undergoes oxidation during the reaction process to produce molecular nitrogen[27] as a byproduct, reaction (2). The oxidation of the reducing agent is a key step in the overall reaction mechanism, where it plays a role in facilitating the reaction with the metal center and the formation of AlN.

Because $HN(CH_3)_2$ is detected during both TDMAA and NH_3 pulses, (Fig. 4a and b) while CH_4 is only detected during the NH_3 pulse (Fig. 5b), it is reasonable to assume that CH_4 evolves as either a ligand decomposition (illustrated later in reaction (7)),[19] or a reductive elimination product, that has possibly undergone hydrogenation reactions upon interaction with NH_3,[32] which acts as an atomic H source and this reaction pathway can be illustrated as follows:

$$\|\text{–}N_2AlN(CH_3)_2^\bullet + 4H^\bullet \rightarrow \|\text{–}N_2AlNH_2^\bullet + 2HN(CH_3)_2(g) + 2CH_4(g) \quad (3)$$

It is worthwhile to note that it's difficult to conclude if the detected signal at m/z = 16 is CH_4^+, NH_2^+ or a combination of both.

4.1.2. Intermediate species. When dimethylamine radicals ($N(CH_3)_2^\bullet$) from the main reaction products are released into the gas phase, they can potentially undergo a disproportionation reaction,[15] resulting in DMA ($HN(CH_3)_2$) and MMI ($CH_2{=}N{-}CH_3$) which were both observed at m/z = 45/44 and 43 respectively, and illustrated by reaction (4).

$$N(CH_3)_2^\bullet + N(CH_3)_2^\bullet \rightarrow HN(CH_3)_2(g) + CH_2{=}N{-}CH_3(g) \quad (4)$$

Dimethylamine radicals can also produce CH_3N (observed at m/z = 29) and methyl radicals (m/z = 15) upon collision with charged particles, reaction (5). Methyl radicals that can recombine to form ethane (m/z = 30). Dimethylamine can further decompose[19] to $HN{=}CH_2$ (m/z = 29) and methane (m/z = 16)

during the plasma process, illustrated by reaction (7) and shown in Fig. 5 for TDMAA and CH_4 in Fig. 7(a) and (b) for TDMAT.

$$N(CH_3)_2^{\bullet} \rightarrow N\text{–}CH_3 + CH_3^{\bullet} \quad (5)$$

$$CH_3^{\bullet} + CH_3^{\bullet} \rightarrow C_2H_6(g) \quad (6)$$

$$HN(CH_3)_2 \rightarrow HN{=}CH_2(g) + CH_4(g) \quad (7)$$

Additionally, mass spectral data indicates the presence of β-hydride elimination mechanisms if we consider that m/z = 43 ($CH_2{=}N\text{–}CH_3$) corresponds to the products from the β-hydride elimination reaction as shown by previous TDMAT studies,[11,19,20,25–27] further split off[36] giving out methane (m/z = 16) and HCN (m/z = 27) as follows:

$$CH_2{=}N\text{–}CH_3 \rightarrow CH_4(g) + HCN(g) \quad (8)$$

This scenario underscores the dynamic characteristics and complexity of alkylamido based chemical reactions and the various pathways that may unfold when their active radicals are introduced into a gas-phase setting.

It is important to acknowledge that the presence of plasma necessitates consideration of dissociation and recombination reactions, as they may have a significant impact on the deposition process.[37] Furthermore, dimethylamine radicals can participate in reductive coupling and elimination reactions[38] leading to the formation of tetramethylhydrazine, highlighting their further potential role in the complex gas phase chemistry.

$$N(CH_3)_2^{\bullet} + N(CH_3)_2^{\bullet} \rightarrow (CH_3)_2N\text{–}N(CH_3)_2(g) \quad (9)$$

The recombination of two dimethylaminyl radicals to produce tetramethylhydrazine is a potential reaction pathway, that has been seen in other alkylamino precursor reaction mechanism studies.[21] However, tetramethylhydrazine was not detected as a product in our study. We assume that the formation of a hydrazine from the reductive coupling of two amido ligands in the TDMAA molecule is hindered when NH_3 is introduced into the reaction mixture. Instead, the presence of NH_3 promotes the reductive elimination by hydrogenation of the dimethylamido ligands,[21] leading to the production of the corresponding amine, which in this case is DMA. This phenomenon can be explained by NH_3 acting as a competing reactant or coordinator in the reaction system. NH_3 may interact with the Al metal center or the ligands, altering the reaction pathway and favoring the hydrogenation process over the reductive coupling to form hydrazine. As a result, the formation of hydrazine is suppressed, and more dimethylamine is produced due to the increased hydrogenation of the amido ligands. In a way, the presence of NH_3 influences the reaction selectivity by shifting the equilibrium towards the hydrogenation pathway, thereby affecting the overall product distribution in the decomposition and reactivity of TDMAA.

4.1.3. Overall mechanism. The proposed reaction and film growth mechanisms between TDMAA and NH_3 from observed signals is illustrated in Fig. 8. The unprotonated and protonated ligand with m/z = 44 and 45 detected during the TDMAA pulse suggest that the first half reaction of TDMAA on the presumably –NH_2 terminated surface is a ligand exchange whereas the second half cycle is a transamination reaction resulting in the protonation and release of the ligand which can possibly decompose in the gas phase, forming a variety of intermediate species, and retaining the initial NH_2-terminated surface.

4.2. Reaction kinetics

A kinetic analysis of the reaction with NH_3 on a TDMAA terminated surface by an Arrhenius analysis is shown in Fig. 9:

From Fig. 9, activation barriers were calculated using the Arrhenius equation, which connects the rate constant of a reaction to temperature and activation energy. The Arrhenius equation is expressed as:

$$k = A \cdot e^{-(E_a/RT)}$$

where k is the rate constant, A is the pre-exponential factor, E_a is the activation energy, R is the gas constant, and T is the

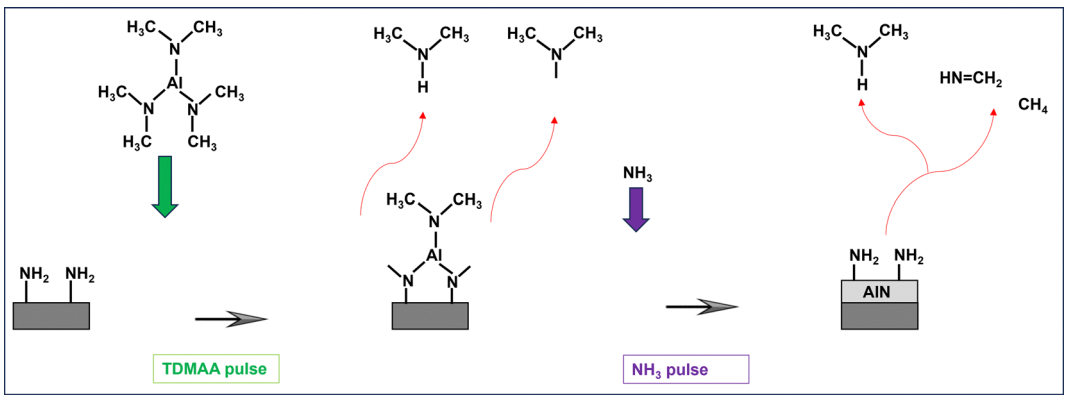

Fig. 8 An illustration of the AlN ALD showing TDMAA reacting with an NH_2-terminated surface, emitting protonated and unprotonated dimethylamine gas from two of the protonated ligands, leaving the surface terminated in aluminum dimethylamide, completing the first half of the reaction. In the second half, the introduced ammonia removes the surface bound dimethylamide as dimethylamine gas that can also undergo ligand decomposition releasing methane and other intermediates, retaining the initial NH_2-terminated surface. With purging in between, this completes one ALD cycle, and the process can be repeated any number of times to achieve the desired thickness.

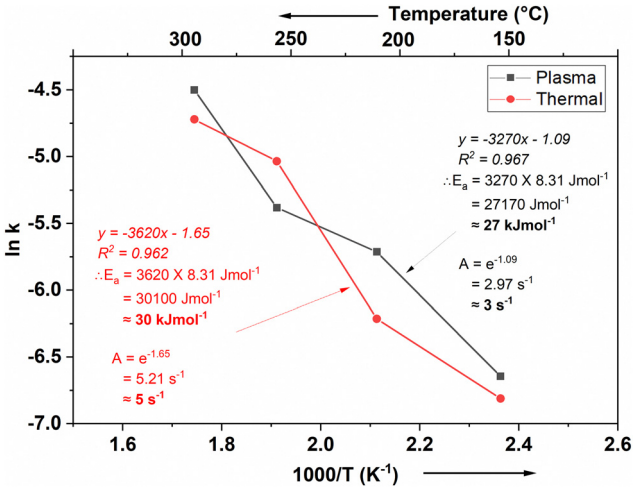

Fig. 9 Arrhenius plot for NH_3 reaction on a TDMAA-terminated surface, emitting dimethylamine, in plasma (black line) and thermal (red line) processes, during the NH_3 pulse. Straight lines (not shown) represent a weighted linear fit to the data, from which the corresponding Arrhenius parameters were drawn.

temperature in Kelvin. To extract activation barriers from experimental data, we conducted kinetic measurements at different temperatures, monitoring changes or decay in partial pressure over time to determine the rate constants. By plotting the natural logarithm of the rate constants ($\ln k$) against the inverse temperature ($1/T$), a linear relationship was observed, allowing us to calculate the activation energy from the slope of the Arrhenius plot. The slopes and intercepts reveal activation energy and frequency factor values at the different temperature regimes. The activation energy is around 27 kJ mol^{-1} and 30 kJ mol^{-1} while the frequency factor is around 3 s^{-1} and 5 s^{-1} for the plasma and thermal process respectively, during the NH_3 half reaction on a TDMAA-terminated surface.

5. Conclusions

We utilized mass spectrometry to investigate the reaction mechanisms involved in plasma and thermal ALD of AlN using $Al(NMe_2)_3$ and NH_3. The formation of different gaseous molecules was demonstrated by the different m/z values detected, and the reaction products during the growth of AlN were identified. The QMS pattern was dominated by $HNMe_2$-related species. Several reactions were observed including the expected hydrogenation to dimethylamine, β-hydride elimination to *N*-methyl methyleneimine, decomposition to methane and hydrogen cyanide. During the exposure to $Al(NMe_2)_3$, the detection of the reaction product $HNMe_2$ indicated its interaction with the surface groups formed from the NH_3 ambient, leading to the detection of $HNMe_2$ and CH_4, mainly formed during transamination exchange and hydrogenation-reduction reactions respectively, and $CH_2{=}NMe$ through disproportionation reactions, as the main reaction products. NH_3 plasma exposure resulted in the presence of molecular nitrogen and further ligand fragmentation, thereby limiting the expected ligand dissociation and radical combination reactions. NH_3 molecules within the plasma also triggered transamination exchange reactions, leading to the generation of the anticipated reaction product, $HN(CH_3)_2$. A comparison with the well-studied TDMAT–NH_3 process showed similarities, leading us to conclude that the reaction of $Al(NMe_2)_3$ with NH_3 falls into the general class of metal nitride deposition processes known as transamination reactions.

Author contributions

Pamburayi Mpofu: conceptualization, data curation, methodology, investigation, formal analysis, visualization, writing – original draft. Houyem Hafdi: conceptualization, methodology, writing – review & editing. Jonas Lauridsen: supervision, formal analysis, writing – review & editing. Oscar Alm: conceptualization, writing – review & editing. Tommy Larsson: supervision, conceptualization, writing – review & editing. Henrik Pedersen: supervision, conceptualization, project administration, funding acquisition, writing – review & editing.

Data availability

The data supporting this article have been included as the ESI.†

Conflicts of interest

The authors declare no conflict of interest.

Acknowledgements

Seco Tools and the Swedish foundation for Strategic Research through the project ''Time-resolved low temperature CVD for III-nitrides'' (SSF-RMA 15-0018) are gratefully acknowledged for financial support. H. P. acknowledges financial support from the Swedish Government Strategic research Area in Materials Science on Advanced Functional Materials at Linköping University (Faculty Grant SFO-Mat-LiU No. 2009-00971).

References

1 H.-E. Nieminen, *Reaction Mechanism Studies on Atomic Layer Deposition Processes*, University of Helsinki, 2024, Vol. Dissertati.
2 X. Fu, Aluminum Nitride Wide Band-Gap Semiconductor and Its Basic Characteristics, 6th International Conference on Electronic, Mechanical, Information and Management Society (EMIM 2016), 2016, 555–558.
3 H. O. Pierson, *Handbook of Chemical Vapor Deposition (CVD)-Principles, Technology, and Applications*, New Jersey, 2nd edn, 1999, vol. 5.
4 D. Riihelä, M. Ritala, R. Matero, M. Leskelä, J. Jokinen and P. Haussalo, Low Temperature Deposition of AlN Films by an Alternate Supply of Trimethyl Aluminum and Ammonia, *Chem. Vap. Depos*, 1996, **2**, 277–283.

5 P. Mpofu, H. Hafdi, P. Niiranen, J. Lauridsen, O. Alm, T. Larsson and H. Pedersen, Surface Chemistry in Atomic Layer Deposition of AlN Thin Films from $Al(CH_3)_3$ and NH_3 Studied by Mass Spectrometry, *J. Mater. Chem. C*, 2024, **12**, 12818–12824.
6 P. Rouf, P. Sukkaew, L. Ojamäe and H. Pedersen, Reduction of Carbon Impurities in Aluminum Nitride from Time-Resolved Chemical Vapor Deposition Using Trimethylaluminum, *J. Phys. Chem. C*, 2020, **124**, 14176–14181.
7 S. C. Buttera, D. J. Mandia and S. T. Barry, Tris(Dimethylamido)Aluminum(iii): An Overlooked Atomic Layer Deposition Precursor, *J. Vac. Sci. Technol., A*, 2017, **35**, 01B128.
8 K. H. Kim, R. G. Gordon, A. Ritenour and D. A. Antoniadis, Atomic Layer Deposition of Insulating Nitride Interfacial Layers for Germanium Metal Oxide Semiconductor Field Effect Transistors with High-κ Oxide/Tungsten Nitride Gate Stacks, *Appl. Phys. Lett*, 2007, **90**, 2005–2008.
9 A. I. Abdulagatov, R. R. Amashaev, K. N. Ashurbekova, K. N. Ashurbekova, M. K. Rabadanov and I. M. Abdulagatov, Atomic Layer Deposition of Aluminum Nitride and Oxynitride on Silicon Using Tris(Dimethylamido)Aluminum, Ammonia, and Water, *Russ. J. Gen. Chem.*, 2018, **88**, 1699–1706.
10 E. Eisenbraun and A. E. Kaloyeros, Ultrathin Diffusion Barriers/Liners For Gigascale Copper Metallization, *Annu. Rev. Mater. Sci.*, 2000, **30**, 365–385.
11 J. N. Musher and R. G. Gordon, Atmospheric Pressure Chemical Vapor Deposition of TiN from Tetrakis-(Dimethylamido)Titanium and Ammonia, *J. Mater. Res.*, 1996, **11**, 989–1001.
12 J. P. A. M. Driessen, J. Schoonman and K. F. Jensen, Infrared Spectroscopic Study of Decomposition of $Ti(N(CH_3)_2)_4$, *J. Electrochem. Soc.*, 2001, **148**, G178–G184.
13 L. H. Dubois, B. R. Zegarski and G. S. Girolami, Infrared Studies of the Surface and Gas Phase Reactions Leading to the Growth of Titanium Nitride Thin Films from Tetrakis-(Dimethylamido)Titanium and Ammonia, *J. Electrochem. Soc.*, 1992, **139**, 3603–3609.
14 E. T. Norton and C. Amato-wierda, Kinetic and Mechanistic Studies of the Thermal Decomposition of $Ti(N(CH_3)_2)_4$ during Chemical Vapor Deposition by *in Situ* Molecular Beam Mass Spectrometry, *Chem. Mater.*, 2001, **13**, 4655–4660.
15 S. Salim, C. K. Lim and K. F. Jensen, Gas-Phase Decomposition Reactions of Tris(Dimethylamino)Phosphine, -Arsine, and -Stibine Reagents, *Chem. Mater.*, 1995, **7**, 507–516.
16 R. G. Gordon, ALD Precursors and Reaction Mechanisms, *At. Layer Depos. Semicond.*, 2014, **9781461480**, 15–46.
17 R. L. Puurunen, Surface Chemistry of Atomic Layer Deposition: A Case Study for the Trimethylaluminum/Water Process, *J. Appl. Phys*, 2005, **97**, 121301.
18 R. L. Puurunen and W. Vandervorst, Island Growth as a Growth Mode in Atomic Layer Deposition: A Phenomenological Model, *J. Appl. Phys*, 2004, **96**, 7686–7695.
19 C. M. Truong, P. J. Chen, J. S. Corneille, W. S. Oh and D. W. Goodman, Low-Pressure Deposition of TiN Thin Films from a Tetrakis(Dimethylamido)Titanium Precursor, *J. Phys. Chem.*, 1995, **99**, 8831–8842.
20 D. Longrie, D. Deduytsche, J. Haemers, P. F. Smet, K. Driesen and C. Detavernier, Thermal and Plasma-Enhanced Atomic Layer Deposition of TiN Using TDMAT and NH3 on Particles Agitated in a Rotary Reactor, *ACS Appl. Mater. Interfaces*, 2014, **6**, 7316–7324.
21 M. Bouman and F. Zaera, Reductive Eliminations from Amido Metal Complexes: Implications for Metal Film Deposition, *J. Electrochem. Soc.*, 2011, **158**, D524.
22 K. Li, S. Li, N. Li, D. A. Dixon and T. M. Klein, Tetrakis(Dimethylamido)Hafnium Adsorption and Reaction on Hydrogen Terminated Si(100) Surfaces, *J. Phys. Chem. C*, 2010, **114**, 14061–14075.
23 J. Yun, M. Park and S. Rhee, Effect of the Gas-Phase Reaction in Metallorganic Chemical Vapor Deposition of TiN from Tetrakis(Dimethylamido)Titanium, *J. Electrochem. Soc.*, 1998, **145**, 2453–2456.
24 T. Kim and F. Zaera, Surface Chemistry of Pentakis-(Dimethylamido)Tantalum on Ta Surfaces, *J. Phys. Chem. C*, 2011, **115**, 8240–8247.
25 J. Musschoot, Q. Xie, D. Deduytsche, S. Van den Berghe, R. L. Van Meirhaeghe and C. Detavernier, Atomic Layer Deposition of Titanium Nitride from TDMAT Precursor, *Microelectron. Eng.*, 2009, **86**, 72–77.
26 H. K. Kim, J. Y. Kim, J. Y. Park, Y. Kim, Y. D. Kim, H. Jeon and W. M. Kim, Metalorganic Atomic Layer Deposition of TiN Thin Films Using TDMAT and NH_3, *J. Korean Phys. Soc.*, 2002, **41**, 739–744.
27 J. W. Elam, M. Schuisky, J. D. Ferguson and S. M. George, Surface Chemistry and Film Growth during TiN Atomic Layer Deposition Using TDMAT and NH_3, *Thin Solid Films*, 2003, **436**, 145–156.
28 J. C. Hackley, J. D. Demaree and T. Gougousi, Growth and Interface of HfO_2 Films on H-Terminated Si from a TDMAH and H_2O Atomic Layer Deposition Process, *J. Vac. Sci. Technol., A*, 2008, **26**, 1235–1240.
29 W. Chen, Q. Q. Sun, M. Xu, S. J. Ding, D. W. Zhang and L. K. Wang, Atomic Layer Deposition of Hafnium Oxide from Tetrakis(Ethylmethylamino) Hafnium and Water Precursors, *J. Phys. Chem. C*, 2007, **111**, 6495–6499.
30 T. R. Cundari and J. M. Morse, Decomposition Pathways for a Model TiN Chemical Vapor Deposition Precursor, *Chem. Mater.*, 1996, **8**, 189–196.
31 J. C. F. Rodrıguez and A. V. Teplyakov, Surface Transamination Reaction for Tetrakis (Dimethylamido) Titanium with NHX-Terminated Si(100) Surfaces, *J. Phys. Chem. C*, 2007, **111**, 16498–16505.
32 L. H. Dubois, Model Studies of Low Temperature Titanium Nitride Thin Film Growth, *Polyhedron*, 1994, **13**, 1329–1336.
33 H. Kim, C. Detavenier, O. Van Der Straten, S. M. Rossnagel, A. J. Kellock and D. G. Park, Robust TaN_x Diffusion Barrier for Cu-Interconnect Technology with Subnanometer Thickness by Metal-Organic Plasma-Enhanced Atomic Layer Deposition, *J. Appl. Phys*, 2005, **98**, 014308.
34 W. J. Maeng, S.-J. Park and H. Kim, Atomic Layer Deposition of Ta-Based Thin Films: Reactions of Alkylamide Precursor with Various Reactants, *J. Vac. Sci. Technol., B*, 2006, **24**, 2276–2281.

35 S. E. Potts and W. M. M. Kessels, Energy-Enhanced Atomic Layer Deposition for More Process and Precursor Versatility, *Coord. Chem. Rev.*, 2013, **257**, 3254–3270.
36 H. Fujiwara, T. Egawa and S. Konaka, Electron Diffraction Study of Thermal Decomposition Products of Trimethylamine: Molecular Structure of CH_3NCH_2, *J. Mol. Struct.*, 1995, **344**, 217–226.
37 H. C. M. Knoops, E. Langereis, M. C. M. van de Sanden and W. M. M. Kessels, Reaction Mechanisms of Atomic Layer Deposition of TaN_x from $Ta(NMe_2)_5$ Precursor and H_2-Based Plasmas, *J. Vac. Sci. Technol., A*, 2012, **30**, 01A101.
38 F. Zaera, The Surface Chemistry of Atomic Layer Deposition (ALD) Processes for Metal Nitride Film Growth, *ECS Meet. Abstr.*, 2010, 1412.